ADVANCED MATERIALS
www.advmat.de



# Polarization-Mediated Thermal Stability of Metal/Oxide Heterointerface

*Qintong Zhang, Lu You, Xi Shen, Caihua Wan, Zhonghui Yuan, Xuan Zhang, Li Huang, Wenjie Kong, Hao Wu, Richeng Yu, Junling Wang,* and Xiufeng Han**

With great advances in thin-film growth and characterization techniques, heterointerfaces are rising as rich grounds hosting various emergent phases of condensed matters as well as exotic functionalities inaccessible in the corresponding bulk materials.[1–5] Aside from the structurally commensurate epitaxial oxide interfaces where multiple degrees of freedom (spin, orbital, charge, and lattice) are intimately linked, the hybrid interfaces between metals and oxides are also receiving considerable attention from the research community. Among them, hybrid interfaces comprising ferromagnetic metals and ferroelectric/multiferroic oxides are of particular interest for the next-generation magnetoelectric memories, in which magnetism can be tuned electrically via strain-/spin-mediated couplings across the interfaces.[6–11] However, these two constituents are chemically incompatible with each other as oxidation of the metal layer is apt to take place during the fabrication process. Even if a chemically sharp interface can be achieved, subsequent electrical switching can also lead to irreversible oxidation of the ferromagnetic layer, which is detrimental to the device performance.[12] Notable examples include Fe/$BaTiO_3$ heterointerface where a native iron oxide exists[13,14] and CoFe/$BiFeO_3$-based giant magnetoresistance (GMR) device that fails after only a few electric cycles.[15] Hence, it remains a challenge to improve the stability of the metal/oxide heterointerface before it can be incorporated with existing spintronics devices to build the new class of magnetoelectric random access memories (ME-RAM), which take advantages of nondestructive readout as well as low-power electrical writing processes.[16–18]

For spintronics devices, such as magnetic tunneling junctions (MTJs), annealing process is usually indispensible to obtain higher tunneling magnetoresistance (TMR) ratio before MTJs can be applied as magnetic sensors,[19] magnetic read heads, or a storage unit in magnetic random access memories (MRAM).[20] Multistep annealing process is used to achieve linear magnetoresistance in MgO-MTJ sensors.[19] In the case of MRAM, TMR ratio of CoFeB/MgO/CoFeB MTJs can be improved from 20% to 220% after 350 °C annealing process.[20] This thermal treatment, however, will inevitably promote the chemical reaction between oxygen and metal atoms, further deteriorating the interfacial coupling in a ferromagnetic/ferroelectric (multiferroic) heterostructure, and eventually leading to the failure of the GMR or TMR devices. Therefore, the thermal stability of the metal/oxide interface is at the core of the reliability of the interface-mediated magnetoelectric effect, which warrants adequate attention in the recent magnetoelectric renaissance.

Intuitively, the interfacial oxidation process is directly determined by the ionization energies or electronegativities of the metals as well as the cations in the oxides. However, in this communication, we report an unexpected modulation of thermal stability of metal/oxide interface by the spontaneous polarization of the ferroelectric oxide. The mechanism is believed to rest on the inherent coupling between spontaneous polarization and defect chemistry of the ferroelectric oxide via electrostatic interaction.[21,22] This finding casts new insights into the chemistry of the metal/oxide heterointerface, and provides extra degree of principle in device design with better performance.

CoFeB/$BiFeO_3$(BFO) was chosen as the metal/oxide system in this study. Due to the robustness of its multiferrocity at room temperature, BFO has been extensively studied in the past decade, as a promising candidate for magnetoelectric devices. Abundant work has been devoted to study magnetic properties of BFO and its coupling behaviors with adjacent magnetic materials,[23–26] proving the feasibility to control magnetism by electrically tuning the magnitude of exchange bias or switching the magnetic anisotropy of the ferromagnetic layer.[27–30] Amorphous $Co_{40}Fe_{40}B_{20}$ is beneficial to obtain high TMR[31,32] or GMR[13] ratio and can be easily prepared by magnetron sputtering which is widely used in industry. From here onward, CoFeB is used to represent $Co_{40}Fe_{40}B_{20}$. However, all the device paradigms rely critically on the delicate magnetic coupling at the interface, which is highly sensitive to the interface chemistry. Thus, it would be desirable to test the thermal stability of the CoFeB/BFO heterointerface.

During annealing, the thermally activated oxygen ions move into the magnetic layer and form oxides with the magnetic metal. To improve the thermal stability of the CoFeB/BFO

Q. Zhang, Dr. C. Wan, Z. Yuan, X. Zhang, L. Huang, W. Kong, H. Wu, Prof. X. Han
State Key Laboratory of Magnetism
Institute of Physics
Chinese Academy of Sciences
Beijing 100190, China
E-mail: xfhan@iphy.ac.cn
Dr. L. You, Prof. J. Wang
School of Materials Science and Engineering
Nanyang Technological University
639798, Singapore
E-mail: JLWang@ntu.edu.sg
Dr. X. Shen, Prof. R. Yu
Laboratory of Advanced Materials & Electron Microscopy
Institute of Physics
Chinese Academy of Sciences
Beijing 100190, China

**DOI: 10.1002/adma.201502754**

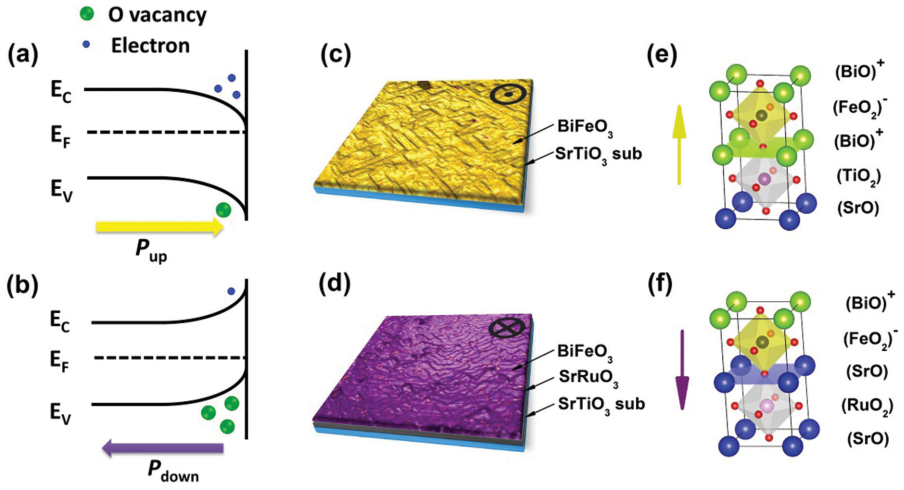


**Figure 1.** Schematic band diagrams of ferroelectric oxide (BFO) layer which is in contact with vacuum during high-temperature growth, whose preset polarization points a) upward and b) downward, respectively. The surface of the ferroelectric layer is indicated by the perpendicular black line. The right side of this line is the vacuum region. Detailed band structures are also shown in Figure S2 in the Supporting Information. Out-of-plane PFM signals overlaid on the topographic images of c) STO(sub.)/BFO and d) STO(sub.)/SRO/BFO demonstrated the direction of spontaneous polarization. In the case of STO(sub.)/BFO and STO(sub.)/SRO/BFO, the polarization points away from the substrate and towards the substrate, respectively. The area of c) and d) is $3 \times 3$ μm$^2$. Schematic diagrams of atomic stacking for e) STO(sub.)/BFO and f) STO(sub.)/SRO/BFO heterointerface.

interface, this oxidation reaction must be suppressed. There are two effective methods to prevent oxidation: i) increasing the density of oxygen vacancies around the surface of BFO and ii) suppressing of the electrochemical oxidation reaction at the interface. **Figure 1**a,b was drawn to illustrate the band structure of BFO which is in contact with vacuum during high-temperature growth. Because the growth temperature is way below BFO's Curie temperature, the BFO is still in its ferroelectric state. Driven by the need to screen the polarization bound charges, oxygen vacancies are preferably formed at the side with negative bound charges, resulting in asymmetric distribution of the oxygen vacancies after the BFO growth. With the help of preset polarization direction, the surface of BFO can be set to oxygen-rich or poor.[33,34] A polarization-mediated surface with poor oxygen distribution could dramatically weaken the oxidation reaction. In addition, band structure of oxide/metal heterointerface also has its influence on this chemistry process which involves a transfer of electrons. When polarization of BFO points downward, the bound charge at the interface is negative. The depolarization field, in opposite direction of polarization, points from the bulk to the interface. The energy of electron at the interface is higher than that of electron located in the body, resulting in the upward bending of conduction and valence bands.[35–37] This upward band bending prevents negatively charged oxygen ions from transferring into the metal layer, and suppresses the oxidation reaction. As a result, the thermal stability of oxide/metal heterointerface could be improved by introducing a downward polarized ferroelectric film which could raise the density of oxygen vacancies and suppress the electrochemical oxidation reaction at the interface.

The topography images of $SrTiO_3$(STO) substrate, $SrRuO_3$(SRO) grown on STO substrate, BFO grown on STO, and BFO grown on STO(sub.)/SRO was demonstrated by Atomic Force Microscope (Supporting Information, Figure S1). The out-of-plane piezoelectric force microscopy (OP-PFM) images shown in Figure 1c,d verifies the opposite alignment of the polarization in STO/BFO and STO/SRO/BFO samples, respectively. This is made possible by controlling the atomic terminations, and accordingly the uncompensated charges of the substrate surface.[38,39] Specifically, as shown in Figure 1e,f, bare STO substrate terminates with $TiO_2$ results in a $TiO_2^0$-$BiO^+$ atomic stacking and consequently a fully $P_{up}$ state (polarization point away from the substrate). In contrast, SRO-coated STO leads to a $SrO^0$-$FeO_2^-$ stacking and a fully $P_{down}$ state (polarization point towards the substrate) due to the A-site termination inversion of the substrate. Spin valves consisting of CoFeB(4)/Cu(2)/Co(4)/$Ir_{22}Mn_{78}$(12)/Ta(5 nm) were grown on top of BFO in these two samples.

The GMR ratio in a spin valve is defined as:

$$\Delta R/R = (R_{AP} - R_P)/R_{AP} \quad (1)$$

where $R_{AP}$ and $R_P$ are the corresponding resistances when the two magnetic layers are antiparallely (AP) or parallely (P) magnetized. In our case, the CoFeB in direct contact with BFO is the free layer, while the upper Co layer adjacent to IrMn is the pinned layer. Below 300 °C, the magnitude of Co/IrMn(12 nm) exchange bias was stable.[40] According to previous reports,[41,42] the oxidation of the free layer reduces the effective magnetic thickness of the free layer, which depresses the spin-dependent bulk scattering effect and thus decreases the GMR effect. When the spin-dependent scattering is depressed, $R_{AP} - R_P$ becomes smaller. So the GMR ratio decreases. Thus, oxidation of CoFeB by oxygen ions from BFO layer during the annealing process would be indirectly reflected by the decrease in GMR ratio. Therefore, spin valves on bare STO(sub.), STO(sub.)/SRO/BFO, and STO(sub.)/BFO are used as probes to explore thermal stability of the interface between BFO and magnetic metal CoFeB.

Typical GMR curve and magnetic hysteresis loop of STO/BFO/STO/BFO/CoFeB(4)/Cu(2)/Co(4)/$Ir_{22}Mn_{78}$(12)/Ta(5 nm)



*Adv. Mater.* **2015**,
DOI: 10.1002/adma.201502754

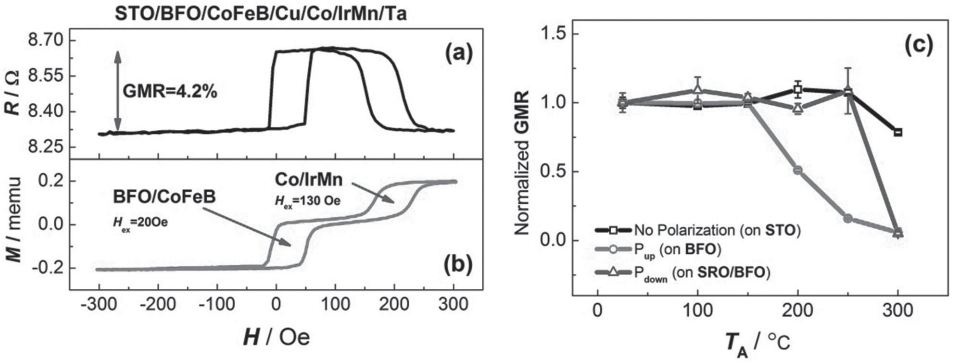


**Figure 2.** a) Giant magnetoresistance curve and b) representative magnetic hysteresis loop of STO/BFO/CoFeB(4)/Cu(2)/Co(4)/$Ir_{22}Mn_{78}$(12)/Ta(5 nm) after 150 °C annealing. Applied magnetic fields in hysteresis and RH measurements were all along the induced easy axis of CoFeB. c) Annealing temperature ($T_A$) dependence of normalized giant magnetoresistance ratio in spin valve grown on STO substrate (squares), STO (sub.)/BFO (circles), and STO (sub.)/SRO/BFO (triangles).

are shown in **Figure 2**a,b, respectively. In the GMR curve, there are two stable resistance states corresponding to antiparallel (high resistance) and parallel state (low resistance) states. First, free layer and pinned layer of the GMR device were both magnetized to saturation negatively, corresponding to the low resistance $R_P$. As increasing the magnetic field positively, the free layer (CoFeB) was switched to the positive direction first and the pinned layer maintained in the negative direction, corresponding to the high resistance $R_{AP}$. Finally, as increasing the magnetic field positively, the pinned layer was switched to positive direction, leading to the low resistance $R_P$. In the hysteresis loop, the same magnetic reversal process is observed as the GMR curve. Both free and pinned layer were negatively magnetized at first. Then free layer and pinned layer were switched to positive one after another as increasing magnetic field positively. The GMR ratio is about 4.2% at room temperature. Coercivity ($H_c$) of the free layer is 30 Oe with a small exchange bias of about 20 Oe. The exchange bias of the pinned layer is about 130 Oe which is quite stable after annealing process.

Magnetoresistance measurements were then performed after 1 h annealing process of different temperatures. The change of the normalized GMR ratio against the annealing temperature is presented in Figure 2c. The GMR ratio of spin valves with upward polarization begins to decrease at an annealing temperature of 150 °C, and almost disappears after 250 °C annealing (see Figure 2c). This reduction of GMR ratio strongly indicates that oxidation occurs through the BFO and CoFeB interface, because the GMR of CoFeB(4)/Cu(2)/Co(4)/$Ir_{22}Mn_{78}$(12)/Ta(5 nm) alone does not decrease even after 250 °C annealing. Oxidation of free layer would also decrease the saturation magnetization ($M_s$) of CoFeB adjacent to BFO and this has been verified by the hysteresis loops (Supporting Information, Figure S3). By contrast, the GMR ratio of the spin valves with downward polarization persists up to 250 °C and only disappears above 300 °C (see Figure 2c). As expected, the downward polarization leads to higher oxygen vacancy density on the BFO surface and suppresses the oxidation reaction between BFO and the adjacent ferromagnetic metal. By tuning the as-grown polarization direction of BFO, the thermal stability of BFO/CoFeB interface is improved by about 100 °C. However, annealing above 300 °C would eventually destroy the device performance due to the onset of decomposition of BFO (Supporting Information, Figure S4).

To investigate the oxidation of CoFeB at the interface, annular bright field (ABF), energy dispersive X-ray spectroscopy (EDS) and electron energy-loss spectroscopy (EELS) experiments were performed using a Cs-corrected transmission electron microscope. As shown in **Figure 3**a for STO/BFO/CoFeB(4)/Cu(2)/Co(4)/$Ir_{22}Mn_{78}$(12)/Ta(5 nm), interdiffusion can be observed and the interfaces become rough after 300 °C annealing process. It is noted that the disappearance of GMR is not merely caused by the rough interface because the GMR value of GMR device grown on STO was close to that GMR of as grown. Main reason is that oxygen ions diffuse into the GMR multilayers and lead to magnetic metal oxidization. This concentration gradient of oxygen ions is demonstrated in EDS results (in Figure 3b). In Figure 3b, oxygen element is observed throughout the BFO and STO substrate and begins to decrease in GMR multilayers in oxidized sample. To confirm this observation, EELS spectra of Co and oxygen in the GMR multilayers including Co and CoFeB are acquired.[43,44] In the upper Co layer which is adjacent to IrMn (Figure 3d1), only EELS spectrum of Co-$L_{2,3}$ edges could be acquired. The spectrum of oxygen is negligible. However, in the bottom Co which is adjacent to Cu, EELS spectra of Co-$L_{2,3}$ and O-K edges are both observed (Figure 3d2). It indicates that partial Co element in Co layer is also oxidized by oxygen ion from BFO. During the annealing process, Co element in CoFeB layer is oxidized by oxygen ions (Figure 3c). In the Co EELS spectra of the CoFeB layer (Figure 3e), $L_3/L_2$ ratio shows that both $Co^{2+}$ and $Co^{3+}$ exist, indicating that CoO and $Co_3O_4$ might form during the annealing process. CoO is antiferromagnetic and $Co_3O_4$ is paramagnetic at room temperature, both of which would result in decrease of the saturation magnetization (Supporting Information, Figure S3).

In summary, we have investigated the thermal stability of GMR devices on ferroelectric BFO films. It is observed that the BFO polarization direction induced oxygen vacancies difference is the key to the change in thermal stability of the metal/oxide heterointerface. Through polarization engineering, the thermal stability of the interface between BFO and CoFeB can be improved by about 100 °C. The oxidation at the interface

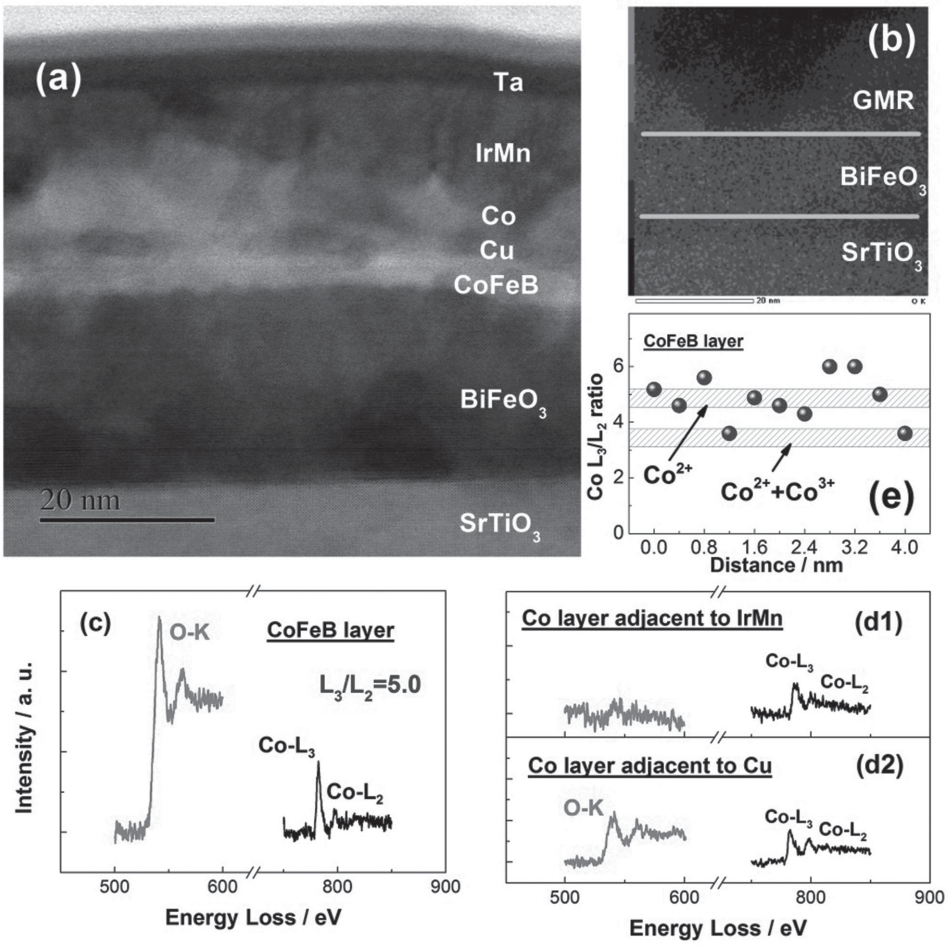


**Figure 3.** a) The cross-section ABF image of STO/BFO/CoFeB(4)/Cu(2)/Co(4)/$Ir_{22}Mn_{78}$(12)/Ta(5 nm) after 300 °C annealing. b) EDS mapping of oxygen element in STO/BFO/GMR (not the same area as (a) but the same sample). c) EELS spectra of O-K edge and Co-$L_{2,3}$ edge in CoFeB layer with subtraction of the background. d1) EELS spectra of O-K and Co-$L_{2,3}$ in Co layer adjacent to IrMn without oxidation. d2) EELS spectra of O-K and Co-$L_{2,3}$ in Co layer adjacent to Cu with partial oxidation. e) Profiles of EELS $L_3/L_2$ intensity ratios of Co in the CoFeB layer (scan step is 0.4 nm).

between BFO and GMR multilayers is confirmed by combining scanning transmission electron microscopy and EELS with macroscopic magnetic characterizations. This work could be helpful to introduce annealing process to BFO/FM interface while maintain the magnetic properties of ferromagnetic layer, and the development of electrically tunable GMR or TMR devices for memory applications.

## Experimental Section

20 nm thick $SrRuO_3$ bottom electrode was grown on (001)-oriented $SrTiO_3$ single crystal substrate by pulsed laser deposition (PLD) at 650 °C. Subsequently, about 40-nm-thick epitaxial $BiFeO_3$ film was fabricated on $SrTiO_3$ single crystal substrate and SRO-coated $SrTiO_3$ substrate at 650 °C using a stoichiometric $BiFeO_3$ target. BFO films were grown at 13 Pa oxygen pressure and in situ annealed to room temperature in oxygen atmosphere at $10^4$ Pa for 2 h. Surface topography and ferroelectric domain images were studied using PFM based on an atomic force microscope system (Asylum Research MFP-3D). After that, we prepared GMR multilayers on epitaxial BFO films using ULVAC magnetron sputter system with a base pressure of $2.0 \times 10^{-6}$ Pa under magnetic field of 200 Oe. Spin valve consists of $Co_{40}Fe_{40}B_{20}$(4)/Cu(2)/Co(4)/$Ir_{22}Mn_{78}$(12)/Ta(5 nm). Magnetic properties of GMR multilayers were measured by vibrating sample magnetometer (Microsense, EZ7) at room temperature. Measurement electrodes of four-probe method were achieved by combined ultraviolet optical lithography technique and Ar-ion beam etching. Magnetoresistance tests were carried out by Keithley 2400 and 2182 in a Helmholtz coils system at room temperature. Annealing process was carried out in a vacuum system with a base pressure of $10^{-4}$ Pa and a static magnetic field of 5 kOe. Sample was heated to the target temperature at the rate of 5 °C $min^{-1}$, held for 1 h and cooled down to room temperature. Further investigation on the interface structure was carried out by cross-sectional STEM, EDS, and EELS experiments using JEM-ARM200F (JEOL).

## Supporting Information

Supporting Information is available from the Wiley Online Library or from the author.

## Acknowledgements

The project was supported by the State Key Project of Fundamental Research and 863 Plan Project of Ministry of Science and Technology




DOI: 10.1002/adma.201502754

[MOST, Grant No. 2010CB934401], the MOST National Key Scientific Instrument and Equipment Development Projects [Grant No. 2011YQ120053], and National Natural Science Foundation of China [NSFC, Grant Nos. 11434014 and 51229101]. L.Y. and J.W. acknowledge support from the Ministry of Education, Singapore under project MOE2013-T2–1–052.

Received: June 9, 2015
Revised: July 30, 2015
Published online:

[1] J. Mannhart, D. G. Schlom, *Science* **2010**, *327*, 1607.
[2] P. Zubko, S. Gariglio, M. Gabay, P. Ghosez, J.-M. Triscone, *Annu. Rev. Condens. Matter Phys.* **2011**, *2*, 141.
[3] J. Chakhalian, A. J. Millis, J. Rondinelli, *Nat. Mater.* **2012**, *11*, 92.
[4] H. Y. Hwang, Y. Iwasa, M. Kawasaki, B. Keimer, N. Nagaosa, Y. Tokura, *Nat. Mater.* **2012**, *11*, 103.
[5] P. Yu, Y.-H. Chu, R. Ramesh, *Mater. Today* **2012**, *15*, 320.
[6] C.-G. Duan, S. S. Jaswal, E. Y. Tsymbal, *Phys. Rev. Lett.* **2006**, *97*, 047201.
[7] V. Garcia, M. Bibes, L. Bocher, S. Valencia, F. Kronast, A. Crassous, X. Moya, S. Enouz-Vedrenne, A. Gloter, D. Imhoff, C. Deranlot, N. D. Mathur, S. Fusil, K. Bouzehouane, A. Barthélémy, *Science* **2010**, *327*, 1106.
[8] T. H. E. Lahtinen, J. O. Tuomi, S. van Dijken, *Adv. Mater.* **2011**, *23*, 3187.
[9] S. Valencia, A. Crassous, L. Bocher, V. Garcia, X. Moya, R. O. Cherifi, C. Deranlot, K. Bouzehouane, S. Fusil, A. Zobelli, A. Gloter, N. D. Mathur, A. Gaupp, R. Abrudan, F. Radu, A. Barthélémy, M. Bibes, *Nat. Mater.* **2011**, *10*, 753.
[10] T. H. E. Lahtinen, K. v. J. A. Franke, S. van Dijken, *Sci. Rep.* **2012**, *2*, 258.
[11] S. Zhang, Y. G. Zhao, P. S. Li, J. J. Yang, S. Rizwan, J. X. Zhang, J. Seidel, T. L. Qu, Y. J. Yang, Z. L. Luo, Q. He, T. Zou, Q. P. Chen, J. W. Wang, L. F. Yang, Y. Sun, Y. Z. Wu, X. Xiao, X. F. Jin, J. Huang, C. Gao, X. F. Han, R. Ramesh, *Phys. Rev. Lett.* **2012**, *108*, 137203.
[12] S. Couet, M. Bisht, M. Trekels, M. Menghini, C. Petermann, M. J. Van Bael, J.-P. Locquet, R. Rüffer, A. Vantomme, K. Temst, *Adv. Funct. Mater.* **2014**, *24*, 71.
[13] L. Bocher, A. Gloter, A. Crassous, V. Garcia, K. March, A. Zobelli, S. Valencia, S. Enouz-Vedrenne, X. Moya, N. D. Mathur, C. Deranlot, S. Fusil, K. Bouzehouane, M. Bibes, A. Barthélémy, C. Colliex, O. Stéphan, *Nano Lett.* **2011**, *12*, 376.
[14] G. Radaelli, D. Petti, E. Plekhanov, I. Fina, P. Torelli, B. R. Salles, M. Cantoni, C. Rinaldi, D. Gutiérrez, G. Panaccione, M. Varela, S. Picozzi, J. Fontcuberta, R. Bertacco, *Nat. Commun.* **2014**, *5*. 3404.
[15] J. T. Heron, J. L. Bosse, Q. He, Y. Gao, M. Trassin, L. Ye, J. D. Clarkson, C. Wang, J. Liu, S. Salahuddin, D. C. Ralph, D. G. Schlom, J. Iniguez, B. D. Huey, R. Ramesh, *Nature* **2014**, *516*, 370.
[16] C. Binek, B. Doudin, *J. Phys.: Condens. Matter* **2005**, *17*, L39.
[17] M. Bibes, A. Barthelemy, *Nat. Mater.* **2008**, *7*, 425.
[18] J. Allibe, S. Fusil, K. Bouzehouane, C. Daumont, D. Sando, E. Jacquet, C. Deranlot, M. Bibes, A. Barthélémy, *Nano Lett.* **2012**, *12*, 1141.
[19] J. Y. Chen, J. F. Feng, J. M. D. Coey, *Appl. Phys. Lett.* **2012**, *100*, 142407.
[20] S. S. P. Parkin, C. Kaiser, A. Panchula, P. M. Rice, B. Hughes, M. Samant, S.-H. Yang, *Nat. Mater.* **2004**, *3*, 862.
[21] E. Breckenfeld, A. B. Shah, L. W. Martin, *J. Mater. Chem. C* **2013**, *1*, 8052.
[22] A. R. Damodaran, E. Breckenfeld, Z. Chen, S. Lee, L. W. Martin, *Adv. Mater.* **2014**, *26*, 6341.
[23] C. Ederer, N. A. Spaldin, *Phys. Rev. B* **2005**, *71*, 060401(R).
[24] X. Ke, P. P. Zhang, S. H. Baek, J. Zarestky, W. Tian, C. B. Eom, *Phys. Rev. B* **2010**, *82*, 134448.
[25] L. W. Martin, Y. H. Chu, M. B. Holcomb, M. Huijben, P. Yu, S-J. Han, D. Lee, S. X. Wang, R. Ramesh, *Nano Lett.* **2008**, *8*, 2050.
[26] D. Sando, A. Agbelele, D. Rahmedov, J. Liu, P. Rovillain, C. Toulouse, I. C. Infante, A. P. Pyatakov, S. Fusil, E. Jacquet, C. Carrétéro, C. Deranlot, S. Lisenkov, D. Wang, J.-M. Le Breton, M. Cazayous, A. Sacuto, J. Juraszek, A. K. Zvezdin, L. Bellaiche, B. Dkhil, A. Barthélémy, M. Bibes, *Nat. Mater.* **2013**, *12*, 641.
[27] T. Zhao, A. Scholl, F. Zavaliche, K. Lee, M. Barry, A. Doran, M. P. Cruz, Y. H. Chu, C. Ederer, N. A. Spalidin, R. R. Das, D. M. Kim, S. H. Baek, C. B. Eom, R. Ramesh, *Nat. Mater.* **2006**, *5*, 823.
[28] Y. H. Chu, L. W. Martin, M. B. Holcomb, M. Gajek, S. J. Han, Q. He, N. Balke, C. H. Yang, D. Lee, W. Hu, Q. Zhan, P-L. Yang, A. Fraile-Rodriguez, A. Scholl, S. X. Wang, R. Ramesh, *Nat. Mater.* **2008**, *7*, 478.
[29] J. T. Heron, M. Trassin, K. Ashraf, M. Gajek, Q. He, S. Y. Yang, D. E. Nikonov, Y-H. Chu, S. Salahuddin, R. Ramesh, *Phys. Rev. Lett.* **2011**, *107*, 217202.
[30] D. Lebeugle, A. Mougin, M. Viret, D. Colson, L. Ranno, *Phys. Rev. Lett.* **2009**, *103*, 257601.
[31] D. Wang, C. Nordman, J. Daughton, Z. Qian, J. Fink, *IEEE Trans. Magn.* **2004**, *40*, 2269.
[32] D. D. Djayaprawira, K. Tsunekawa, M. Nagai, H. Maehara, S. Yamagata, N. Watanabe, S. Yuasa, Y. Suzuki, K. Ando, *Appl. Phys. Lett.* **2005**, *86*, 092502.
[33] S. V. Levchenko, A. M. Rappe, *Phys. Rev. Lett.* **2008**, *100*, 256101.
[34] Y. M. Kim, A. Morozovska, E. Eliseev, M. P. Oxley, R. Mishra, S. M. Selbach, T. Grande, S. T. Pantelides, S. V. Kalinin, A. Y. Borisevich, *Nat. Mater.* **2014**, *13*, 1019.
[35] S. Dunn, P. M. Jones, D. E. Gallardo, *J. Am. Chem. Soc.* **2007**, *129*, 8724.
[36] D. Conklin, T.H. Park, S. Nanayakkara, M. J. Therien, D. A. Bonnell, *Adv. Funct. Mater.* **2011**, *21*, 4712.
[37] B. C. Huang, Y. T. Chen, Y. P. Chiu, Y. C. Huang, J. C. Yang, Y. C. Chen, Y. H. Chu, *Appl. Phys. Lett.* **2012**, *100*, 122903.
[38] P. Yu, W. Luo, D. Yi, J. X. Zhang, M. D. Rossell, C.-H. Yang, L. You, G. Singh-Bhalla, S. Y. Yang, Q. He, Q. M. Ramasse, R. Erni, L. W. Martin, Y. H. Chu, S. T. Pantelides, S. J. Pennycook, R. Ramesh, *Proc. Natl. Acad. Sci. USA* **2012**, *109*, 9710.
[39] Y. C. Chen, C. H. Ko, Y. C. Huang, J. C. Yang, Y. H. Chu, *J. Appl. Phys.* **2012**, *112*, 052017.
[40] H. N. Fuke, K. Saito, M. Yoshikawa, H. Iwasaki, M. Sahashi, *Appl. Phys. Lett.* **1999**, *75*, 3680.
[41] A. Veloso, P. P. Freitas, P. Wei, N. P. Barradas, J. C. Soares, B. Almeida, J. B. Sousa, *Appl. Phys. Lett.* **2000**, *77*, 1020.
[42] G. C. Han, P. Luo, J. J. Qiu, K. B. Li, Y. H. Wu, *Appl. Phys. A* **2002**, *75*, 655.
[43] D. H. Pearson, C. C. Ahn, B. Fultz, *Phys. Rev. B* **1993**, *47*, 8471.
[44] Z. L. Wang, J. S. Yin, Y. D. Jiang, *Micron* **2000**, *31*, 571.